MULTIAXIAL TESTING OF AERONAUTIC COMPOSITE STRUCTURES 1 MULTIAXIAL TESTING OF AERONAUTIC COMPOSITE STRUCTURES AT INTERMEDIATE SCALE

Bruno Castanié, Jean-Charles Passieux, Jean-Noël Périé, Christophe Bouvet, John-Eric Dufour, Joël Serra

MULTIAXIAL TESTING OF AERONAUTIC COMPOSITE STRUCTURES AT INTERMEDIATE SCALE

Bruno Castanié[1], Jean-Charles Passieux[1], Jean-Noel Périé[1], Christophe Bouvet[1], John-Eric Dufour[1], Joël Serra[1]

[1]Institut Clément (ICA), Université de Toulouse, CNRS UMR 5312, INSA, ISAE-Supaéro, INSA, IMT Mines Albi, UPS, France

Abstract

The certification of aeronautical composite structures is based on a pragmatic approach, which is intended to be safe and essentially experimental but with a strong test/calculation dialogue called the “Test Pyramid”. However, this has proved to be extremely expensive and it appears necessary to reduce its cost either by developing Virtual testing, or by developing richer tests on an intermediate scale between coupon specimens and structural parts. It was in the aim of meeting this objective that the VERTEX program (French acronym for “Experimental modeling and Validation of compositE strucTures under complEX loading”) was launched in 2012. After positioning the VERTEX program in relation to the literature, this paper will explain the methodology and present three scientific themes that have been studied will be detailed (large notches, impact and wrinkling case studies). Finally, a proposal for validating the structures using envelope curves will be put forward, an assessment made, and perspectives presented.

Keywords: Testing; Multiaxial loading; Composite Structures; Large notches; Wrinkling.

1. General Introduction

The certification of aeronautical composite structures is based on a pragmatic approach, which is intended to be safe. It is essentially experimental but uses a strong test/calculation dialogue called the “Test Pyramid” (Fig. 1, [1,2]). The first level of the pyramid is that of coupon tests, which make it possible to obtain the admissible values for the current sections, the junctions and the impact, considering the environmental effects (temperatures and humidity) and also the dispersion (A values and B values). At higher levels, the structural details, then the subassemblies and, finally, the complete aircraft must be validated. It can also be noted that these tests are uniaxial, while the structures are subjected to multiaxial constraints. In total, several tens of thousands of tests are carried out during programs such as those of the BOEING 787 or the AIRBUS A350. The costs associated with this approach are very high and generate very long design cycle times. In addition, many problems can only be detected during late structural tests, and thus generate significant additional costs. There is therefore a need to develop a standard testing methodology at scales greater than coupons but without going into the complexity of the structural details [3]. This is what we will call the intermediate scale. In addition, deep knowledge of the structural response early in the aircraft program makes it possible to develop and make digital models that will become more reliable by being part of a Virtual Testing Approach. A literature review of various testing bench technologies that make it possible to satisfy this need have already been presented in [4] and [5] and will not be recalled here. The design comes from the past experience on the testing of asymmetric sandwich structures [6, 7]. In the following section, the operating principle of the machine and the main points of development will be recalled. In this type of structure, it may be interesting to know the direct relationship between the forces applied and the stresses in the specimen. Such a transfer law has recently been found via an explicit nonlinear modeling of the assembly and the findings will be presented briefly. The specific measurement methods developed for the VERTEX test bench can be found in a summary in [3] and [4].

The Vertex test bench was used to study many issues linked to composite aeronautic structures, in cooperation with industry, thus avoiding full scale tests: large notches on thermoplastic and thermoset panels, with Airbus [4, 8, 9], combined loading after impact, with Segula Aerospace & Defence [10, 11], wrinkling of sandwich panels, with Elixir Aircraft [12, 13, 14], debonding of stiffeners, with Airbus [15] and very recently buckling tests on wooden sandwich structures with Avions Mauboussin. Then two case studies, i.e. large notches and impact will be presented. A paragraph is then dedicated to the concept of failure envelopes, which are allowed by this means of testing. The paper will conclude with a succinct presentation of current studies, an assessment of the contribution of the VERTEX method, and perspectives.

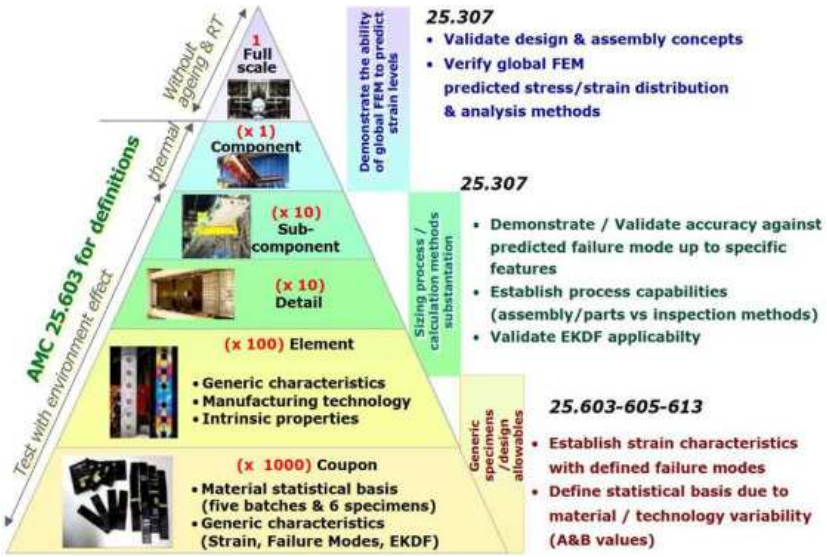

Figure 1 – The pyramid of tests [1] representing the numerous small mechanical tests providing a design basis for fewer and larger tests [2] (Courtesy of Airbus).

2. The VERTEX test bench

The specifications after a benchmark with aeronautics manufacturers made it possible to establish a maximum load envelope: 3000 N/mm in traction or compression, 1000 N/mm in shear, and an internal pressure of 1.6 bars. The principle of the machine is shown in Figs. 2 and 3. The specimen is bolted onto the upper part of the central box located between the two IPN transversal beams. When jacks 1 and 2 are activated, the whole longitudinal box is subjected to 4-point bending and therefore the specimen can be loaded under tension or compression. When jacks 3 and 4 are activated, the central box is twisted and the sample is thus subjected to shear. Of course, these four jacks can also be used in combinations.

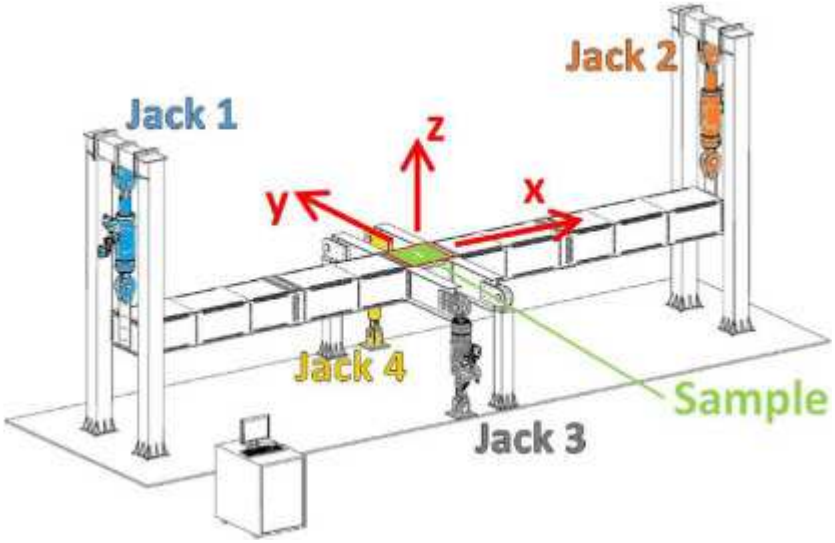

Figure 2 – Principle of combined loading with the VERTEX test bench.

By comparison to the first generation [6, 7], the area of interest was quadrupled to 400×400 mm^2, which typically corresponds to the size of one or two bays (the inter-frame and inter-stiffener areas). The laboratory has a large reaction table on which the assembly could be fixed but which imposes space constraints. The details of the sizing and load cases are given in [4] and the final assembly can be seen in Fig. 4.

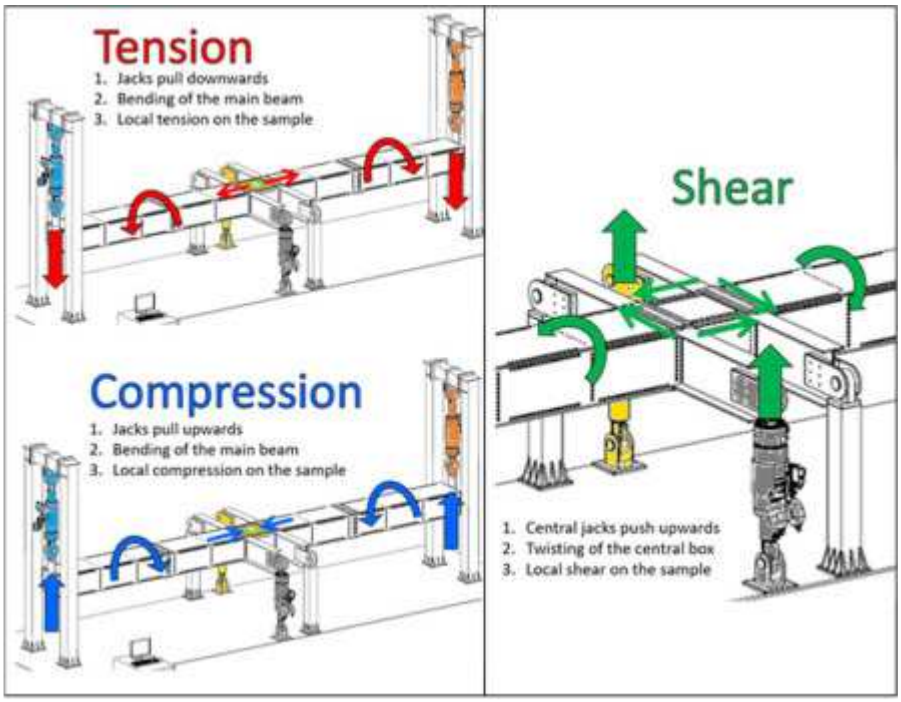

Figure 3 – Actuation of the four jacks of the VERTEX test rig to deform the bench and locally apply tension/compression and shear to the sample.

Figure 4 – Overview of the VERTEX test bench.

The overall dimensions are 8.5 m length, 2.9 m width and 3 m height. The box itself is 0.5 m high. 128 bolts are used to fasten the specimen on the central box and to sustain the maximum loads (Fig. 5(a)), which leads to an overall size of the specimen, including the bolting area, of 558 mm × 536 mm. An air-pressurized rubber bladder (Fig. 5(b)) can be added in the central box to load the sample with pressure. The cost of this assembly (studies, manufacture and assembly) was about 500 k€. Recently [5], a significant effort was made to obtain a comprehensive model of the test bench because a detailed FEM is needed to determine the link between the displacements of the four actuators and

the load (amplitude and shape) actually applied to the specimen. This difficulty is not specific to the VERTEX machine; it occurs every time a large test rig is used. Therefore, the modeling strategy to simulate the behavior of a complex test rig (choice of type of finite elements, connections, contact, solver) has been described. More specifically, attention was paid to the modeling of the bolted joint, especially between the specimen and the VERTEX test bench. The relative influences of the stiffnesses (axial/radial) of the junctions of the machine according to their location (Sample/Box/Beam) have been obtained and an explanation of the internal coupling observed (transverse compression associated with longitudinal tension when “tension” jacks 1–2 are used and the longitudinal tension associated with shear when “shear” jacks 3–4 are used) is provided. Now this explicit model allows us to predict:

- •The bearing loads,
- • The sample shape to delay secondary corner failures and failure assessment using a simple strain criterion.
- • The response of the sample for complex loading paths
- •The sizing of new specimens like impacted stiffened panels [15].

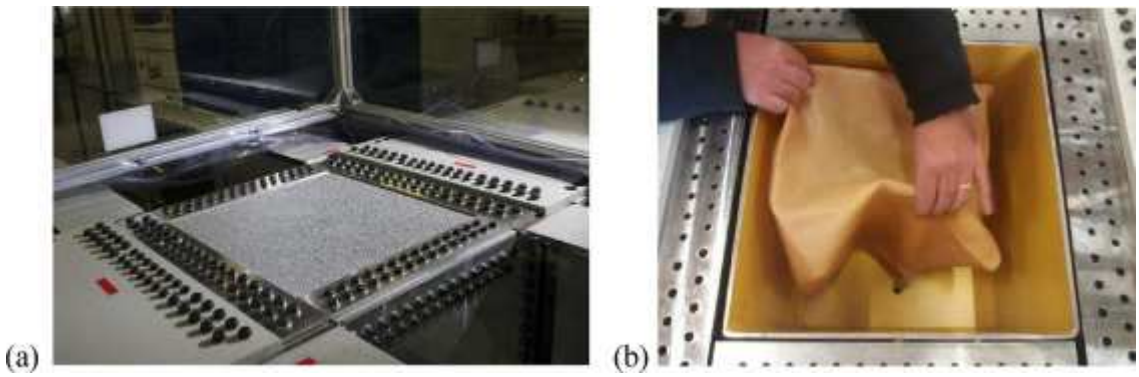

Figure 5 – Zoom on the bolted area of the sample with 128 bolts (a) and on the air-pressurized rubber bladder (b).

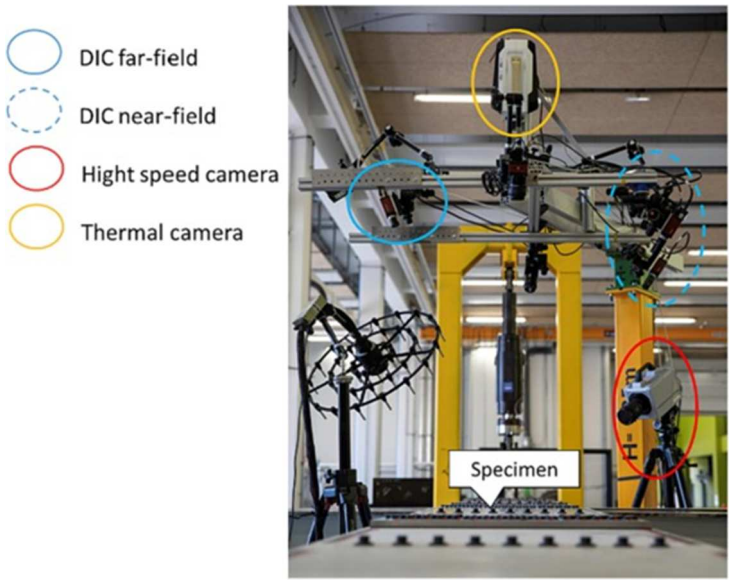

Figure 6 – Measurement devices associated with Vertex tests.

Specific measurement strategy was developed based mainly on FE-SDIC (Finite Element-Stereo digital Image Correlation) which enables a consistent experiment/calculation method using the same finite element mesh for FE-SDIC solution and specimen modeling. Among other capabilities, using classical plate theory and full-field measurements of the stereo-correlation, force fluxes and moment fluxes can be computed from: upper-skin strain measurements, out-of-plane displacement measurements, and the assumed stiffness of the plate. It was therefore possible to compute the

strains in the hidden face of the specimen, showing a very good correlation with strain gages [4, 16]. Typical tests at these intermediary scales are also highly instrumented with in general three pairs of DIC camera, high speed camera and thermal camera to capture the failure scenario (see figure 6 and [4]).

3. Case Study 1: Notched plates

Today, the structures of civil passenger aircraft must be certified as having demonstrated their ability to withstand an exceptional event, such as an uncontained engine explosion, which can create significant damage to a fuselage (see Fig. 7(a) &(b)). Such an in-flight incident can generate a large notch in the fuselage, which may be contained in a bay (skin alone between stringers and frames) or may cut through a stiffening member (frame or stiffener). Most of the time, the sizing of a fuselage according to this criterion is performed with a very expensive test at scale one (see Fig. 7(c)). On the other hand, the residual strength in presence of crack damage of CFRP structures is generally evaluated through the point-stress or similar methods in open-hole tests [20, 21].

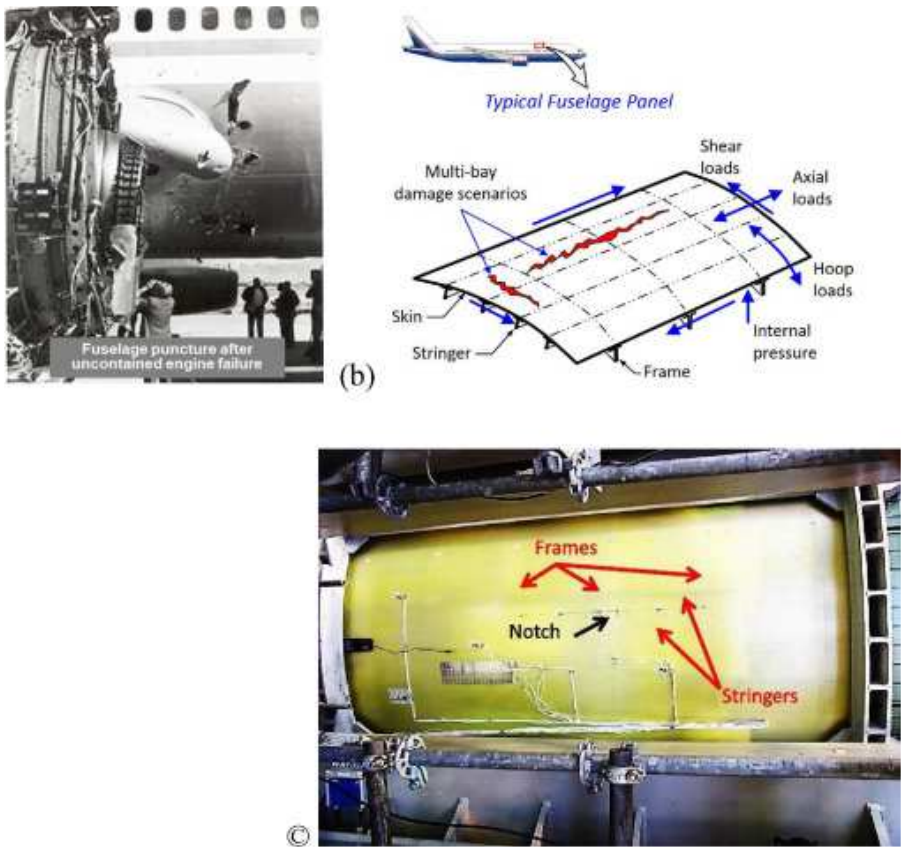

Figure 7: Large damage on fuselage generated by uncontained engine failure ((a) from [18], (b) from [19], (c): Large notch panel full scale test (Courtesy of Airbus).

In notch tests, coupons tend to fail directly and catastrophically, whereas, in larger samples, the crack propagates more progressively. Therefore, the VERTEX system provides boundary conditions and multiaxial loadings which are closer to the real structures but at lower cost compared to full scale tests as in Fig. 7(c). A typical VERTEX specimen (see Fig. 19) was milled to create a 100 mm center-notch to keep the ratio W/L = 4 and to maintain representativeness of large damage phenomenology. The notch was machined with a 2 mm mill. This process left an end notch radius of 1 mm. Unidirectional fibers and thermoset or thermoplastic resin were used in prepeg form. For confidentiality reasons, the exact material reference, the material properties, the thickness and the manufacturing processes of some of the materials used cannot be disclosed in this article. First, the influence of the stacking sequence was studied with prepegs made of Hexcel's T700-M21 carbon epoxy unidirectional laminate with a nominal thickness of 0.125 mm. Two specimens were also manufactured with a double thickness ply of 0.250 mm. Three symmetrical stacking sequences of

13 plies were studied. The three different stackings (C3–1, C3–2, C3–3) presented the same number of plies in each direction (0, 90 and ±45), and only the relative position of the plies changed between layups. X's are used to avoid disclosing the orientations of some plies:

– C3–1 [45/45/X/X/X/90/0/90/X/X/X/45/45]
– C3–2 [X/X/X/X/0/90/0/90/0/X/X/X/X]
– C3–3 [X/X/X/X/X/0/0/0/X/X/X/X/X]

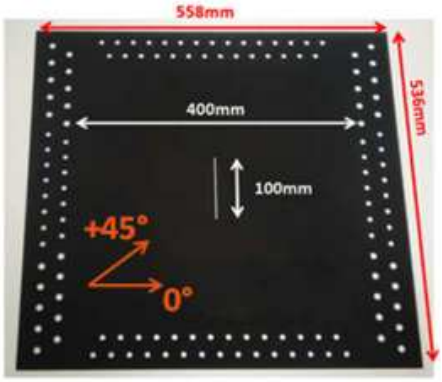

Figure 8: Notched VERTEX specimen geometry.

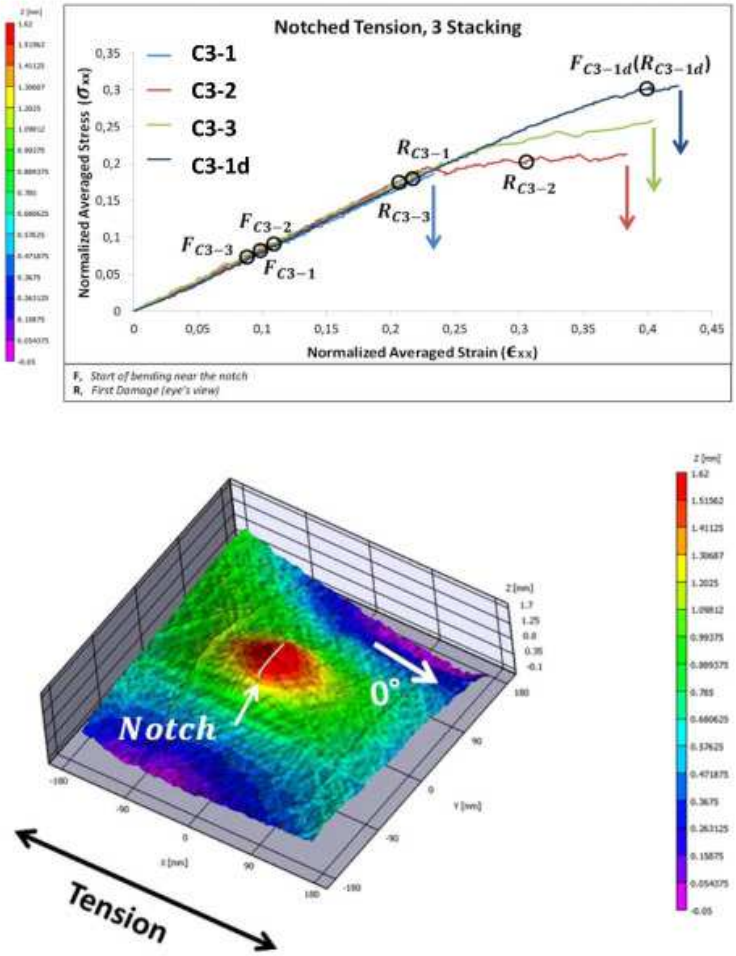

Figure 9. Influence of the stacking sequence and thickness on the notched tensile behavior, (b) Bending around the notch - FC3 – 1 for C3–1 stacking sequence.

Stress/strain curves obtained in tension using the methodology explained in [3] are shown in Fig. 9. The vertical arrows represent the final failure of the laminates, corresponding to cuts that propagated to the edges of the test piece. Using the in-situ measurement, linear curves were obtained until the

damage occurred. In this way, the phases of initial positioning and the possible non-linearities of the assembly were filtered. The specimens were of the same stiffness, 38 GPa, close to the 43 GPa determined experimentally on a notched coupon [20]. This decrease in stiffness was due to the ratio of notch width to specimen width, which was higher for VERTEX (1/4) specimens than for coupon-scale (1/6) specimens.

Localized bending was observed near the notch (Fig. 9, Layout C3–1). It accelerated the propagation of the crack and thus reduced the maximum failure stress. F points correspond to a maximum deflection of the notch border approximately equal to the thickness of the laminate (single thickness: 1.625 mm). The same reference (1.625 mm) was used (in value) for laminates C3–1d This double thickness laminate, being stiffer in bending, required a higher load to reach a similar deflection. The failure stress observed for the double thickness specimen was therefore greater than those observed for the ‘‘single thickness”. The C3–3 specimen showed higher resistance to damage propagation and the failure stress of C3–1, double sized version, was increased even more. Both stacking sequence and thickness effect were therefore identified. C3–1, C3–2 and C3–3 were also tested in shear and tension+shear. More recently, the influence of pressure on tensile, shear and combined tension+shear tests have been investigated (Fig. 10 and [9]). Additional pressure seems to have a slight influence, mainly on the appearance of the first fiber failure detected with an Infrared Camera.

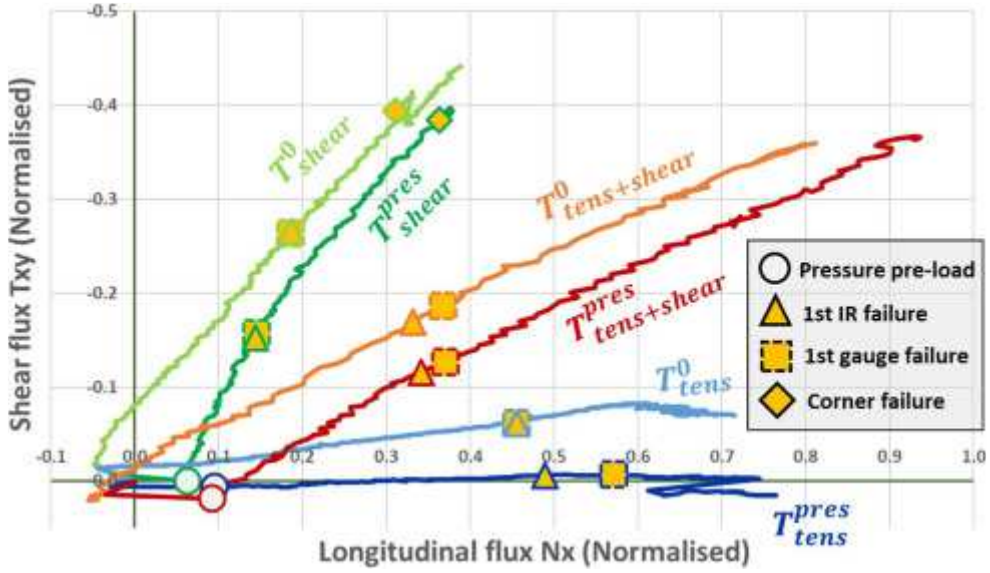

Figure 10. Superposition of computed force flux for each test considered.

4. Case Study 2: testing of impacted plates.

CFRP composite structures are particularly vulnerable to low energy impacts. This leads to a policy of impact damage tolerance and sizing which in turn leads to overweight. These low energy impacts, for example due to unexpectedly dropping of tools [21, 22], can occur in service, during ground operations or in aircraft manufacturing. Even if the damage due to impact is not detectable by visual inspection, the residual resistance of the composite structure can decrease by more than 50 % [21 -24]. The most critical loading case acting on a real aeronautical structure is compression loading, so experimental tests are performed on small coupons of size 100×150 mm^2 in order to certify and size the aeronautical composite structures. Past experience has shown that the allowable values determined by this methodology are conservative. Thus, in order to be less detrimental and to be more representative of the real life of the composite structure, the loss of residual strength after impact should be evaluated at the level of the structural element. This is one of the main advantages of the Vertex test bench. Therefore, an experimental study was performed with the Vertex machine in order to evaluate the loss of residual strength after impact of composite panels with a size more representative of the structural element level [10, 11]. For this size of panel, the important points are the boundary conditions and the postbuckling. Contrary to the situation observed with classical coupons of 100×150 mm^2, where the postbuckling is almost non-existent (which is logical because

the objective is to evaluate the loss of residual strength on the allowable in compression), considerable postbuckling developed during the structural-element-level test: consequently, the residual strength was clearly less influenced by the impact; this result was clearly highlighted during this study, where a unidirectional carbon/epoxy prepreg T700/M21, with a 0.25 mm-thick ply was used. The 14 ply laminate was manufactured with the stacking sequence $[45_2/-45_2/0_2/90]_S$, giving a total thickness of 3.5 mm. Eight specimens were manufactured and tested as mentioned in Table 1: seven were impacted while one was kept unimpacted in order to compare the loss of residual strength, and each underwent a different loading path in the VERTEX test rig.

Table 1: Overview of impact results and loading path

Specimen	***Velocity (m/s)***	***Impact Energy (J)***	***Delaminated Area (mm^2)***	***Loading after Impact***
A	*54*	*40.8*	*5431*	*Compression/shear*
B	*70*	*68.6*	*5239*	*Shear*
C	*75*	*78.7*	*2720*	*Shear/tension*
D	*90*	*113.4*	*9087*	*Compression/shear*
E	*98*	*134.4*	*9842*	*Compression*
F	*100*	*140*	*10091*	*Shear/tension*
G	*110*	*169.4*	*15000*	*Compression*
H	*-*	*-*	*0*	*Shear/tension*

Impact tests were performed with the gas launcher of the Clement Ader Institute impact platform at velocities between 54 and 110 m/s, with a spherical steel impactor 19 mm in diameter and weighing 28 g, which led to impact energies between 40 and 170 J (Table 1). During the impact, the composite panels of 538×400 mm2 size were simply supported by a 400×400 mm^2 impact window (Fig. 11, left). A high-speed camera and a speckled pattern painted on the ball made it possible to evaluate the impactor displacement, velocity and acceleration [25], and thus the impact force. Of course, the higher the energy of the impact, the greater are the maximum displacement and the impact force. Then C-scan investigation was performed on each panel in order to evaluate the delaminated area. Logically, the most delaminated interface was the first interface situated on the non-impacted side, the -45°/45° interface (Fig. 11, right). It should be noted that, compared to classical impact on a small coupon, the extent of the delamination was greater due to the size of the panels and to the significant impact energy levels. This point is interesting because, despite the size of these delaminated areas, it was shown that the loss of residual strength was relatively small, due to the marked post-buckling that developed during the experiments and the hyperstatic clamping of the sample. Then the 8 panels were tested with different loading cases (Table 1), the stress curves for which (σ_{xx}, τ_{xy}) are plotted in Fig. 12. This graph also shows the buckling and the failure. It should be noted that, due to problems of stress concentration in the corners of the plates, most of the final failure started in a corner and propagated in the middle of the plate, at the impact point.

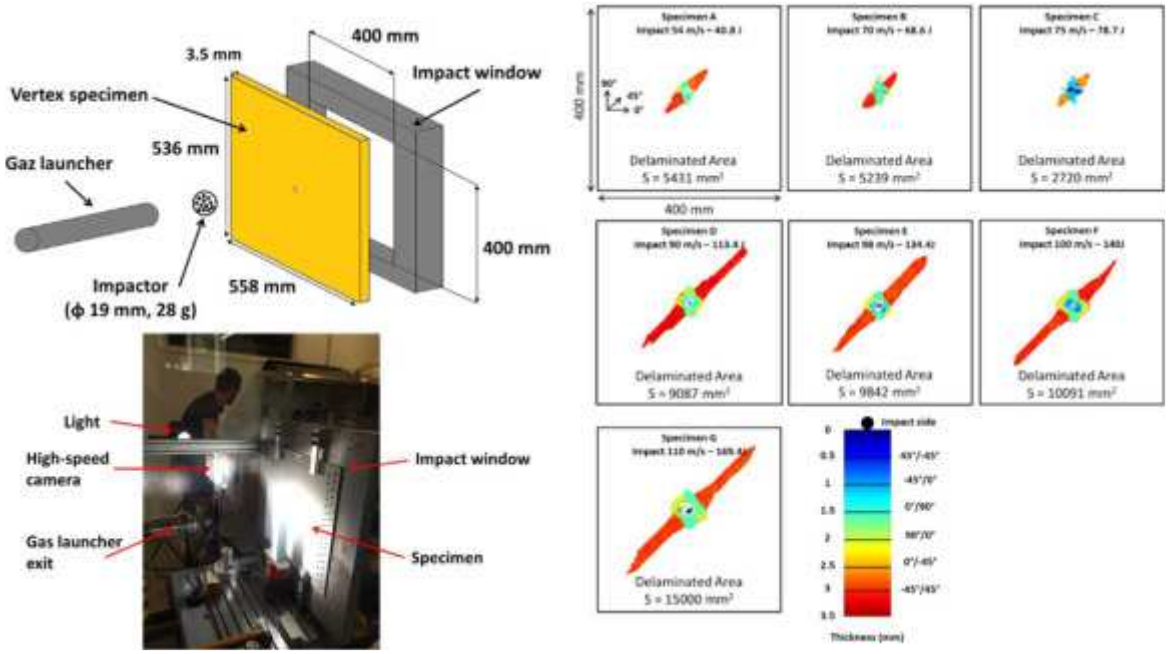

Figure 11. Impact test set-up and Delamination areas obtained by C-Scan after impact for the seven specimens.

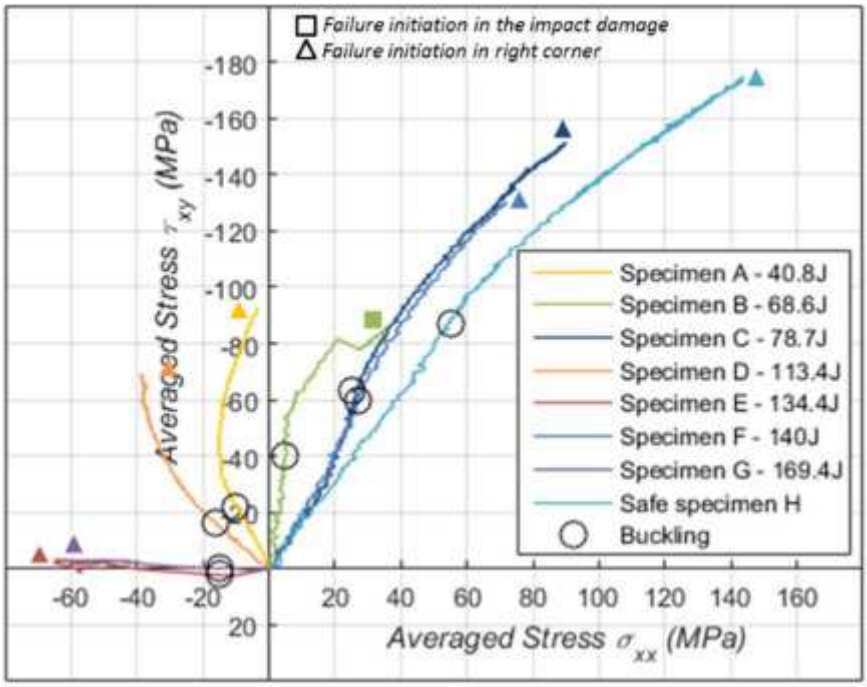

Figure 12. Loading paths for all specimens tested in the VERTEX test rig.

In order to better understand the progression of the experiment, the stress-strain curves of the specimens C, F and H are plotted in Fig. 12. The non-impacted specimen, H, specimen C impacted at 75 m/s and specimen F impacted at 100 m/s (Table 1) were loaded using the torsion actuators 3 and 4, leading to a tension/shear loading path (Fig. 12). This coupling was partly due to the Vertex machine and partly due to the classical tension loading resulting from a shear post-buckling. At the beginning of the test, the stiffnesses of the 3 specimens were similar to one another and similar to the theoretical values. The buckling point logically occurred later for the non-impacted specimen than for impacted specimens and a different loading path was observed for the impacted specimens. It should be noted that, due to the particular concept of the Vertex machine, even if the displacement imposed on the machine is the same, the loading path also depends on the specimen. So, with the same imposed displacement for these 3 samples, the loading paths were slightly different.

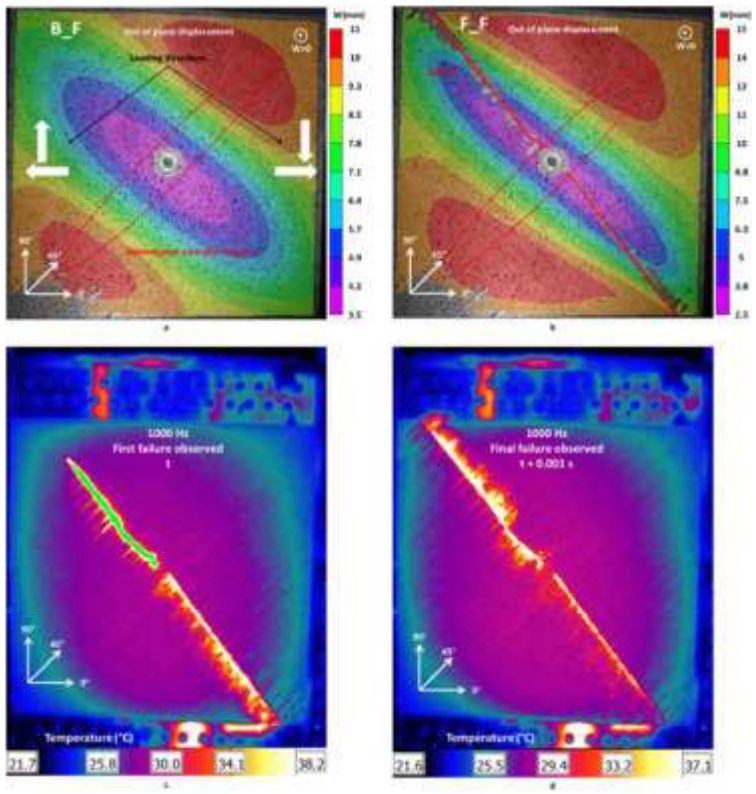

Figure 13. Out-of-plane displacement for specimen F: a – first buckling mode, b – final failure, c – first failure and d – failure propagation observed with thermal camera

The buckling shapes for the 3 samples are similar, with three half waves (Fig. 13), and the final failures are also similar, with the fiber failure of the 45° ply situated on the impacted side and its propagation along the diagonal direction. It is difficult to evaluate the initiation of the final failure because of its high speed (despite the use of the infrared camera) but it seems to have initiated at the bottom right corner of the panel (Fig. 13c). In the first image where the failure is observed (Fig. 13c), then one millisecond before the second image (Fig. 13d; the frame rate of the infrared camera is 1 kHz), the crack has not yet reached the top left corner. Analyzing each loading case individually was crucial for understanding the behavior of each specimen under varying loading conditions. In Fig. 12, we can observe all the loading paths of the specimens along with their corresponding buckling points on a (σ_{xx}, τ_{xy}) graph. It is worth noting that, given the differences in the energy levels at which specimens were impacted, it was not feasible to plot envelope curves for the various impact energy levels. As expected, the compression and compression/shear loading paths emerged as the most critical factors affecting the structure's integrity. In contrast, the tension and tension/shear loading paths tended to mitigate damage propagation. Interestingly, when comparing specimens subjected to the same loading path but impacted at different energy levels (e.g., specimens E and G in pure compression and specimen C in tension/shear), it appeared that the impact damage had minimal influence on the occurrence of buckling but played a significant role in determining the eventual failure. For specimen H, which was not impacted but subjected to the same loading path as specimens C and F, buckling and final failure occurred later in the testing process.

The results obtained indicate that, up to the point of buckling, the impact energy level exerts minimal influence on the specimens. However, an interesting observation is made with the non-impacted specimen H, where buckling occurs later than in specimens subjected to the same loading path. Subsequent to buckling, a noticeable delay is observed in various phenomena (such as mode jump in pure compression loading, initial and final failure) in the most damaged plates. Nevertheless, it appears that the final failure originates from the impact point solely in the pure shear test. In compression, it seems that the impact damage has no discernible effect on the final failure path, which initiates in the bolted zone at the bottom left corner of the specimen. In the cases of compression/shear and tensile/shear loading, thermal camera images suggest that the final failure

initiates in the bottom left corner but is guided by the impact point to propagate along the diagonal of the specimen. Exploring more specimens under compression loading, particularly non-impacted ones, could provide valuable insights into the scale effect on compression after impact. Nevertheless, these initial findings underscore the complexity of the structural response at the scale of an impacted plate, as compared to coupon specimens. Additionally, they highlight the significance of impact location, and it is noteworthy that the current allowances used to size aerospace composite structures may be overly conservative. As elucidated in this paper, one of the main challenges in employing such a test rig is to identify the boundary conditions that affect the specimen. The development and validation of a simplified model for transferring boundary conditions from DIC to Abaqus is a crucial step in enabling the "Virtual Testing" approach to be effectively applied.

5. Envelope curves (non-proportional tests).

The validation of a loading domain, and thus the integrity of the structure to be sized, generally requires many tests because the domain is usually explored with proportional loadings. Serra et al. [8] initially swept the tension-shear domain of loading with envelopes of increasing amplitudes, introducing a safety assessment of the loading domain between the proportional loadings tested previously. The definitions of the envelope tests were based on the results obtained in the proportional tests [8]. This first step was to validate the concept of a safe envelope. In [26], the Safe Life Domain method is formalized and studied in greater depth to validate a whole domain of loading of a given sample, with single envelope testing based on prior simulations and thanks to the VERTEX multi-directional test rig. Fig. 14 illustrates the Safe Life Domain method. Numerical simulations are performed to explore the domain of loading and locate failures – basically by using a failure point for each simulation of proportional loading. The failure points delineate a critical border, which is the frontier between the safe domain and the failed domain. The numerical model developed in [5] is used. A safety margin is taken from the critical border, and a single envelope test is performed along the critical border (Fig. 14). At the end of this envelope test, if the sample is actually safe (no failure detected), then the whole domain of loading encircled is considered safe.

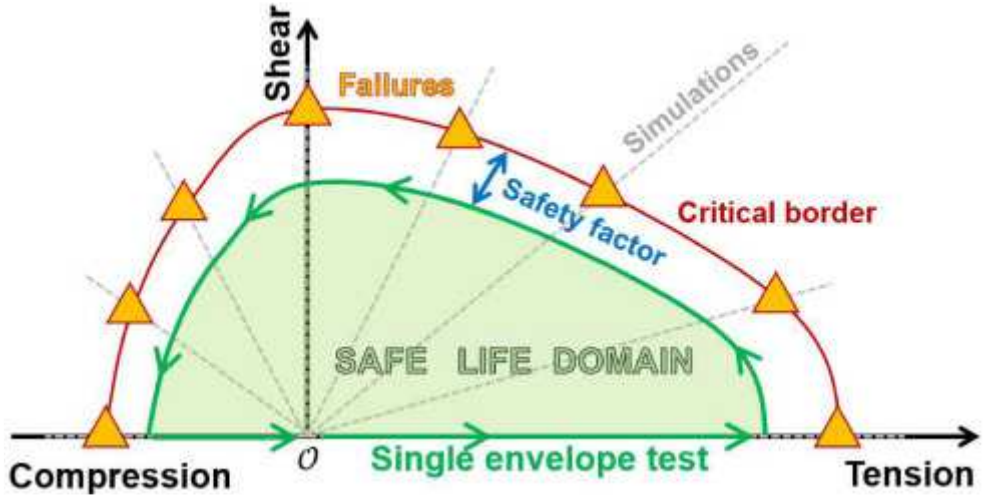

Figure 14. Description of the Safe Life Domain Method to validate a loading domain of a given sample, from numerical simulations and a single envelope test.

The critical border shape depends on:

- The design (flat panel, stiffened panel, sandwich, assembly)
- The material, notably the stacking sequence of a given laminated composite
- The material failure criterion (Yamada-Sun, maximum fiber strain, first fiber failure, etc.)
- The damage type (pristine sample, 100 mm notch, loading after impact, etc.)
- The load shape (pure tension, VERTEX's tension, actual in-situ tension): see previous study for an introduction to the severity and representativeness of loading shapes.

Ultimately, stacked plots of the critical borders of various cases is a matter of great interest for the aeronautical industrial wishing to size structural elements, especially generic panels. Fig. 15 illustrates

nomograms of critical envelopes that could be used to choose materials during the sizing process, depending on the typical load cases to be withstood.

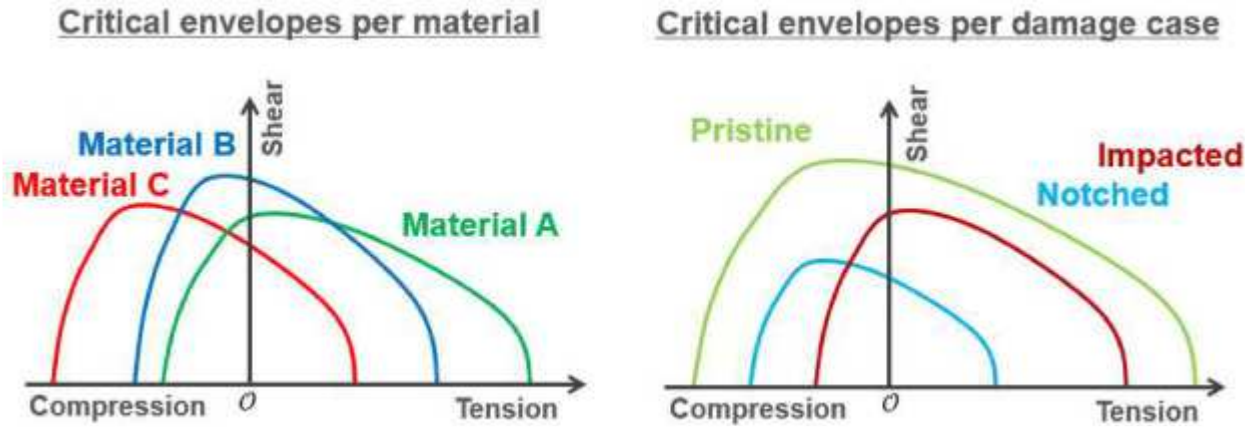

Figure 15. Illustration of stacked critical envelopes on a given specimen – (left) for various pristine materials – (right) for various load cases on a given material.

6. Conclusions.

The VERTEX test bench has demonstrated its capacity and usefulness for testing aeronautical structures, both for light aviation and for large aircraft manufacturers. Large notches, impact and wrinkling of sandwich structures have been presented, whereas ongoing studies have not: postbuckling of impacted single-stiffened structures [20], thermoplastic specimen with large notches and buckling of wood based-sandwich structures. Phenomena and rupture scenarios are different from those of overly simplistic and conservative coupon tests. The complexity is greater, with postbuckling coupled with fracture most of the time, but the phenomena observed are closer to reality and demonstrate that the coupon tests are too conservative, in particular for compression after impact and large notches. The tests are generally highly monitored and specific DIC approaches have been developed to capture the fluxes inside the specimen and even the strains and stress on the hidden faces. This approach also enables an efficient experiment/computation dialog. The possibility of exploring a large area of loading and the validation by a single path through “envelope tests” has also been demonstrated. Today, the test is still on the research side and many efforts are still to be made before it can become a test certified by the aviation authorities

7. References

[1] Rouchon J. Certification of Large Airplane Composite Structures, Recent Progress and New Trends in Compliance Philosophy. *Proc ICAS 17, Stockholm,* pp. 1439-1447, 1990.

[2] Leon-Dufour J-L. Dimensionnement Des Structures Composites Aux dommages. *Journée 3AF CNES*, Toulouse (2008)

[3] Castanié B, Passieux J-C, Périé J-N, Bouvet C, Dufour J-E, Serra J. Multiaxial loading of aeronautic composite structures at intermediate scale: A review of VERTEX developments, *Composites Part C: Open Access*, Vol 13, 100439, 2024.

[4] Serra J, Pierré J-E, Passieux J-C, Périé J-N, Bouvet C, Castanié B. Validation and Modeling of Aeronautical Composite Structures Subjected to Combined Loadings: the VERTEX Project. Part 1: Experimental Setup, FE-DIC Instrumentation and Procedures. *Comp Struct,* Vol 179, pp 224-244, 2017.

[5] Grotto F, Peta O, Bouvet C, Castanié B, Serra J. Testing structural elements under multiaxial loading: a numerical model of the bench to understand and predict complex boundary conditions. *Aerospace,* Vol. 11, No.1, 68, 2024.

[6] Castanié B, Barrau J-J, Jaouen J-P. Theoretical and experimental analysis of asymmetric sandwich structures. *Comp Struct, Vol.* 55, No. 3, pp. 295-306, 2002.

[7] Castanié B, Barrau J-J, Jaouen J-P, Rivallant S. Combined shear/compression structural testing of asymmetric sandwich structures. *Exp Mech*, Vol. 44, No. 5, pp. 461-472, 2004.

[8] Serra J, Pierré J-E, Passieux J-C, Périé J-N, Bouvet C, Castanié B, Petiot C. Validation of aeronautical composite structures under multiaxial loading: the VERTEX Project. Part 2: load envelopes for the assessment of panels with large notches. *Comp Struct*, Vol 180, pp 550-567, 2017.

[9] Grotto F, Bouvet C, Castanié B, Serra J. Experimental behaviour of aeronautical notched carbon fibre

reinforced thermoplastic panels under combined tension-shear-pressure loadings. *Eng Fail Anal*, Vol. 146, 107075, 2023.

[10] Trellu A, Pichon G, Bouvet C, Rivallant S, Castanié B, Ratsifandrihana L. Combined loadings after medium velocity impact on large CFRP laminate plates: Tests and enhanced computation/testing dialogue. *Comp Sci Tech*, Vol. 196, 108194, 2020

[11] Serra J, Trellu A, Bouvet C, Rivallant S, Castanié B, Serra J, Ratsifandrihana L. Combined loadings after medium velocity impact on large CFRP laminated plates: Discrete ply model simulations. *Comp Part C*, Vol. 6, 100203, 2021.

[12] Ginot M, D'Ottavio M, Polit, O, Bouvet C, Castanié B. Benchmark of wrinkling formulae and methods for pre-sizing of aircraft lightweight sandwich structures. *Comp Struct,* Vol. 273, 114387, 2021.

[13] Ginot M, et al. Local buckling on large sandwich panels used in light aviation: Experimental setup and failure scenarios. *Comp Struct*, Vol 304,116439, 2023.

[14] Ginot M, et al. Local buckling on large sandwich panels applied to light aviation: Experimental and computation dialogue. *Int J Sol Struct*, Vol 268, 112170, 2023.

[15] Grotto F, Bouvet C, Castanié B, Serra J. Design and Testing of Impacted Stiffened CFRP Panels under Compression with the VERTEX Test Rig. *Aerospace*, Vol. 10, No. 4, 327, 2023.

[16] Dufour J-E, Colantonio G, Bouvet C, Périé J-N, Passieux J-C, Serra J. Monitoring structural scale composite specimens in a postbuckling regime: the integrated finite element stereo digital image correlation approach with geometrically non-linear regularization. *Strain*, Vol. 59, No. 5, 12450, 2023.

[17] Awerbuch J, Madhukar MS. Notched strength of composite laminates: predictions and experiments—A review. *J Reinf Plast Compos*, Vol. 4, No. 1, pp. 3-159, 1985.

[18] Bazant ZP. *The Scaling of Structural Strength.* HPS, London, 2002.

[19] Camanho PP, Maimí P, Dávila CG. Prediction of size effects in notched laminates using continuum damage mechanics. *Compos. Sci. Technol*, Vol. 67, No. 13, pp 2715-272, 2007.

[20] Serra J, Bouvet C, Castanié B, Petiot C. Experimental and numerical analysis of Carbon Fiber Reinforced Polymer notched coupons under tensile loading. *Comp Struct,* Vol. 148, pp. 127-143, 2016.

[21] Susainathan J, Eyma F, De Luycker D, Cantarel A, Bouvet C, Castanié B. Experimental investigation of compression and compression after impact of wood-based sandwich structures. *Comp Struct,* Vol. 220, pp. 236-249, 2019.

[22] Abrate S, Castanié B, Rajapakse YDS. *Dynamic Failure of Composite and Sandwich Structures.* Springer, 2013.

[23] Tropis A, Thomas M, Bounie JL, Lafon P. Certification of the composite outer wing of the ATR72. *J Aeros Eng Proc Inst Mech Eng Part G,* Vol. 209, pp. 327-339, 1994.

[24] Castanié B, Ginot M, Bouvet C. Review of composite sandwich structure in aeronautic applications. Compos Part C, Vol. 1, 100004, 2020.

[25] Passieux JC, Navarro P, Périé JN, Marguet S, Ferrero JF. A Digital Image Correlation Method For Tracking Planar Motions Of Rigid Spheres: application To Medium Velocity Impacts. *Exp. Mech*, Vol. 54, pp. 1453-1466, 2014.

[26] Grotto F, Bouvet C, Castanié B, Serra J. Numerical simulations and testing of notched composite plates under envelope loadings: validation with the Safe Life Domain method. *Paper submitted to Composite structures, Under revision*.

Copyright Statement